A novel visible light-driven TiO_2 photocatalytic reduction for hexavalent chromium wastewater and mechanism

Baoxiu Zhao, Kaixin Zhang, Yue Huang, Qi Wang, Hao Xu, Yilin Wang, Jincheng Li, Tianwen Song, Wenxiang Xia and Jie Liu

ABSTRACT

Titanium dioxide (TiO_2) photocatalyst was prepared with a sol-gel method and its characterizations were analyzed TiO_2 photocatalytic reduction of Cr^{6+} was investigated in visible light irradiation and reduction mechanisms were calculated. Prepared TiO_2 is anatase with a bandgap of about 2.95 eV. Experimental results display that almost 100% of Cr^{6+} is removed by visible light-driven TiO_2 photocatalytic reduction after 120 min when $Cr_2O_7^{2-}$ initial concentration is 1.0 mg·L^{-1}, TiO_2 dosage is 1.0 g·L^{-1}, and pH value is 3. In acidic aqueous solution, $HCrO_4^-$ is the dominant existing form of Cr^{6+} and is adsorbed by TiO_2, forming a complex catalyst $HCrO_4^-/TiO_2$ with an increase in wavelength to the visible light zone, demonstrated by UV–Vis diffuse reflection spectroscopy. Based on X-ray photoelectron spectroscopy data, it can be deduced that Cr^{6+} is adsorbed on the surface of TiO_2 and then reduced to Cr^{3+} in situ by photoelectrons. Self-assembly of $HCrO_4^-/TiO_2$ complex catalyst and self-reduction of Cr^{6+} in situ are the key steps to start the visible light-driven TiO_2 photocatalytic reduction. Furthermore, TiO_2 photocatalytic reduction of Cr^{6+} fits well with pseudo-first-order kinetics and has the potential application to treat chemical industrial wastewater.

Key words | Cr^{3+}, Cr^{6+}, photocatalytic reduction, TiO_2, visible light

Baoxiu Zhao (corresponding author)
Kaixin Zhang
Yue Huang
Qi Wang
Hao Xu
Yilin Wang
Jincheng Li
Tianwen Song
Wenxiang Xia
Jie Liu
School of Environmental and Municipal Engineering,
Qingdao University of Technology,
Qingdao 266033,
China
E-mail: *zhaobaoxiu@tsinghua.org.cn*

HIGHLIGHTS

- Cr(VI) is efficiently removed by visible light-driven TiO_2 photocatalytic reduction reaction.
- Photoinduced electrons are the major reductive substance for Cr(VI) removal.
- Adsorption, reduction in situ, and desorption are involved in reduction mechanism of Cr(VI).
- Photocatalytic reduction of Cr(VI) fits well with pseudo-first-order kinetics and rate constant is calculated.

GRAPHICAL ABSTRACT

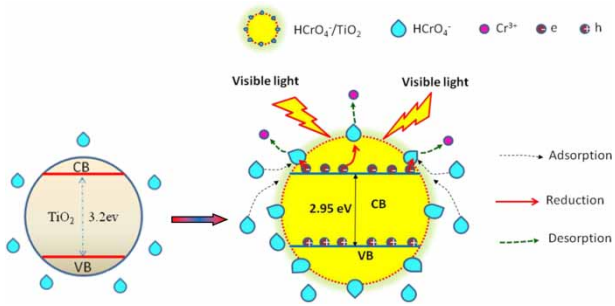

doi: 10.2166/wst.2021.116

INTRODUCTION

Chromium pollutants mainly come from the industries of mining, metallurgy, electroplating, leather manufacture, bichromate, and chromium slag treatment (Zhang *et al.* 2017; Yang *et al.* 2018). However, they are used so widely that many tremendous environmental contaminations (Gheju & Balcu 2017; Ravindra & Mor 2019; Wang *et al.* 2020) are caused. Cr^{6+} is the dominant existing form of chromium compounds and is easily absorbed by bodies. Many international investigations have found that some serious pathological lesions occur not only in the skin (Yu *et al.* 2018) but also in other organs caused when people are exposed to Cr^{6+}-rich environment for a long time (Guo *et al.* 2016; Yoshinaga *et al.* 2018). There are some methods for wastewater containing Cr^{6+}, such as adsorption or biosorption (Deveci & Kar 2013; Vendruscolo *et al.* 2017; Yao *et al.* 2017; Ayub *et al.* 2020), membrane separation (Habibi *et al.* 2015), electrolysis (Sarahney *et al.* 2012), and chemical reagents (Sheikhmohammadi *et al.* 2019). Adsorption is a convenient way for Cr^{6+} removal (Gong *et al.* 2017), but the trace of absorbents should be noticed; otherwise, secondary pollution may be more serious. To avoid the potential risk of absorption, biosorption–biotransformation integrated processes where concentrated Cr^{6+} is reduced to non-toxic Cr^{3+} are developed (Jobby *et al.* 2018). However, the running environment and technical parameters are more strict than those of other technologies. Membrane separation can efficiently remove Cr^{6+} from wastewater; however, membrane assembly is easily contaminated or blocked, and so how to efficiently, safely, and economically remove Cr^{6+} becomes a research focus.

Semiconductor photocatalytic reaction is valued for its powerful redox ability, whether oxidation of most organics (Zhao *et al.* 2016) or reduction of variable valence heavy metal ions. Titanium dioxide (TiO_2) photocatalytic reduction for trace Cr^{6+} has received researchers' attention (Testa *et al.* 2004; Yang *et al.* 2006) for its favorable chemical property, high stability, and low cost (Hoffmann *et al.* 1995). The absorption bandgap of pure TiO_2 ($E_g = 3.2$ eV) lies in the ultraviolet light zone ($\lambda = 1240/E_g = 385$ nm) (Fujishima *et al.* 2008), and it has no ability to oxidize or reduce pollutants in visible light irradiation. TiO_2 modification is a good way to achieve the visible light-driven photocatalytic reaction because the spectrum scope of modified TiO_2 transfers from the ultraviolet light region to the visible light zone. Modified TiO_2 photocatalyst and its application in wastewater treatments have been greatly developed recently. Doping non-ions elements and constructing heterojunctions are both effective methods to achieve TiO_2 photocatalytic performance in visible light irradiation. Chatterjee & Dasgupta (2005) discussed TiO_2 visible light-assisted degradation of organic pollutants and mechanism, and there is more research into TiO_2 photocatalytic degradation for organics in visible light irradiation. The bandgap of TiO_2 doped with elements such as N, F, S, and Bi or anions such as OH^-, SO_4^{2-}, and ClO_4^- becomes narrow, producing a photoelectric response in visible light (Kerkez-Kuyumcu *et al.* 2015; Wang *et al.* 2017). Xu *et al.* (2019) prepared carbon dots (CDs)-modified N–TiO_{2-x} nanocomposite to reduce Cr^{6+} and obtained a satisfied efficiency in visible light irradiation. In addition, p–n junctions can also bring a red shift in the absorption spectrum, exhibiting a powerful visible light response. Magadevan *et al.* (2019) constructed a novel TiO_2–$Cu_2(OH)PO_4$ heterojunction catalyst and found that the composite catalyst exhibited high reduction efficiency of Cr^{6+} because the bandgap narrowed from 3.2 eV to 2.6 eV. Dye-sensitized-TiO_2 also has photocatalytic reduction ability. Wu *et al.* (2013) prepared dye-sensitized TiO_2 to reduce Cr^{6+} under visible light irradiation and found that Cr^{6+} was reduced by photo electrons that diffuse from the dye-sensitized zone to the TiO_2 zone.

There are many investigations into reduction of Cr^{6+} with TiO_2 ultraviolet photocatalysis (Zhou *et al.* 1993) or oxidation for organics with TiO_2 or modified TiO_2 (Asgari *et al.* 2021) or TiO_2-integrated process (Zhao *et al.* 2012, 2015, 2016); however, the study about direct reduction of Cr^{6+} with pure TiO_2 in visible light is scarce. Our previous experiments have shown that in visible light irradiation, Cr^{6+} is reduced to Cr^{3+} by TiO_2 prepared by a sol-gel method. To investigate TiO_2 photocatalytic reduction of Cr^{6+}, process reactions and reduction mechanisms are analyzed in this work.

EXPERIMENTAL

Reagents and chemicals

Titanium butoxide, H_2CrO_4, C_2H_5OH, CH_3COOH, $K_2Cr_2O_7$, HCl, NaOH, and methanol were all analytical degree reagents and purchased from Tianjin Chemical Reagent Co. (China). High pure water (18.2 MΩ·cm^{-1}) was prepared via a water purification instrument (Unique-R20, Research Scientific Instruments Co. Ltd, China).

Synthesis of TiO_2

TiO_2 was prepared via a sol-gel method where titanium butoxide ($Ti(OCH_2CH_2CH_2CH_3)_4$) was used as the precursor. Detailed process is as follows: 100 mL ethanol and 10 mL precursor were mixed together for 20 min at room temperature, forming a homogeneous mixture; 15 mL H_2O and 4 mL CH_3COOH were simultaneously added into the above-mentioned mixture, stirred for 40 min at a constant speed to obtain a mixture with a pH of about 4. The mixture was put into the oven and dried for a set time at 105 °C, to obtain the amorphous TiO_2. Finally, to reach the crystal phase transformation, amorphous TiO_2 was put into a box-type resistance furnace where a gradient temperature was preset. Temperature was raised from room temperature to 250 °C at a heating rate of 5 °C·min^{-1} and kept for 1 h at 250 °C, and then increased from 250 °C to 600 °C at the same heating rate and maintained for 1 h at 600 °C.

Characterization of as-prepared TiO_2

X-ray diffraction (XRD) pattern was monitored by a D/max RB system (Cu Kα_1 irradiation, $\lambda = 1.5406$ Å, voltage = 40 kV, current = 30 mA, scanning rate = 0.01°·s^{-1}, scanning range = 10–80°). Scanning electron microscope (SEM) images were obtained using a Fei Qunta Feg 250 microscope (accelerating voltage = 10 kV). UV–Vis diffuse reflectance spectrum (UV-DRS) was obtained using a UV–Vis diffuse reflectance spectrometer (LAMBDA 750, PerkinElmer) and scanning wavelength range from 200 to 800 nm. X-ray photoelectron spectroscopy (XPS) was controlled by an ESCALAB 250 Xi instrument (ThermoFisher Scientific, Al Kα_1 irradiation, hν = 1486.6 eV, voltage = 12.5 kV, power = 250 W, pressure = 10^{-6}–10^{-7} Pa).

TiO_2 photocatalytic reduction of Cr^{6+}

TiO_2 photocatalytic reduction of Cr^{6+} was conducted in a cylindrical reactor equipped with a 150 W spherical xenon lamp (Shellett Photoelectric Technology Co. Ltd, China). A filter plate was used to remove ultraviolet light and 80 mW·cm^{-1} irradiation intensity was measured using an illumination photometer. Then 200 mL of aqueous solution containing 1.0 mg·L^{-1} $Cr_2O_7^{2-}$ and 1.0 g·L^{-1} TiO_2 powder was transferred into the reactor and stirred at a speed of 100 r·min^{-1} for 60 min, to obtain Cr^{6+} adsorption equilibrium on the surface of TiO_2 and the inside of the reactor in a dark environment. After adsorption equilibrium, the light resource was turned on and photocatalytic reduction was started. Samples were removed from the same place in reactor at given time intervals and the concentration of Cr^{6+} was analyzed using diphenylcarbazide colorimetric method controlled by a UV–Vis spectrophotometer (UV-1900, Shimadzu). Total chromium was analyzed with a graphite furnace atomic absorption spectroscopy (AA4590, Shimadzu).

RESULTS AND DISCUSSION

Characterizations of TiO_2

To determine the crystal phase of as-prepared TiO_2, XRD pattern was performed and results are shown in Figure 1(a)). Compared with the standard anatase TiO_2 (JCPDS: 89-4921), it is observed that the peaks at 2θ of 25.31°, 36.97°, 37.86°, 38.63°, 48.11°, 53.93°, 55.14°, 62.23°, 62.72°,

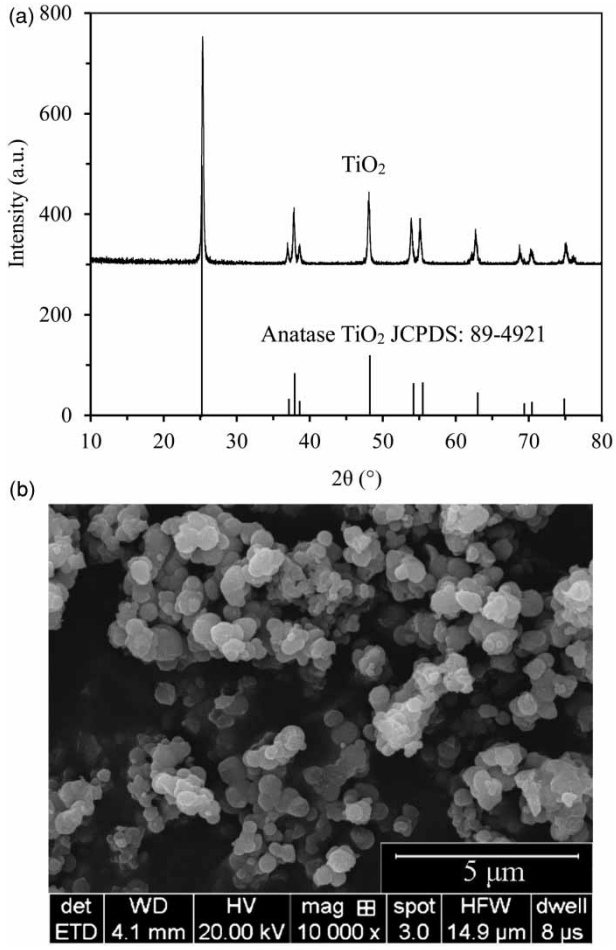

Figure 1 | (a) XRD pattern of TiO_2; (b) SEM image of TiO_2.

68.75°, 70.28°, 75.13°, and 76.15° correspond to (101), (103), (004), (112), (200), (105), (211), (213), (204), (116), (220), (215), and (301) planes of anatase phase, suggesting that as-prepared TiO_2 is clear and perfect, which is in accordance with the research reported by Wang *et al.* (2021). SEM images of as-prepared TiO_2 are shown in Figure 1(b). It seems that TiO_2 looks like some uniform microspheres. The average size of as-prepared TiO_2 is about 78 nm, according to Debye–Scherrer formula ($D = K\lambda/\beta\cos\theta$), where K is a constant of 0.59, λ is irradiation wavelength of 0.15406 nm, β is half-maximum of (101) obtained via XRD software, and θ is the diffraction angle. Furthermore, the surface of TiO_2 is not smooth but layered, which is good for the adsorption and photocatalytic reduction of Cr(VI), compared to the smooth surface.

Effects of TiO_2 dosage and $Cr_2O_7^{2-}$ concentration

The effect of TiO_2 dosage on photocatalytic reduction of Cr^{6+} was investigated and results are displayed in Figure 2(a). It is observed that photocatalytic reduction of Cr^{6+} increases initially and then decreases with the enhancement of TiO_2, and the optimum is 1.0 g·L^{-1}. The reason is that when TiO_2 dosage is lower than 1.0 g·L^{-1}, more Cr^{6+} ions are adsorbed on the TiO_2 surface with the enhancement of catalyst dosage, resulting in high reduction; however, when the dosage is higher than 1.0 g·L^{-1}, the homogeneous solution becomes murky with the increase in catalyst dosage, leading to a reflection of light, meaning that only the surface layer Cr^{6+} aqueous solution receives light irradiation, resulting in low photocatalytic reduction efficiency.

The effect of $Cr_2O_7^{2-}$ concentration on photocatalytic reduction of Cr^{6+} was studied and results are shown in Figure 2(b). It can be seen that reduction efficiency decreases with the enhancement of $Cr_2O_7^{2-}$ concentration. Reduction of Cr^{6+} climbs to 98% at 90 min when $Cr_2O_7^{2-}$ initial concentration is 0.5 mg·L^{-1}; however, it is only 24% when the $Cr_2O_7^{2-}$ initial concentration is 5.0 mg·L^{-1}. The decline of reduction is mainly caused by light scattering. The higher the $Cr_2O_7^{2-}$ initial concentration, the darker the aqueous solution becomes, and then the $Cr_2O_7^{2-}$ anions participating in photocatalytic reduction reduces for the serious scattering of visible light.

Effect of pH

The effect of pH on photocatalytic reduction of Cr^{6+} was studied under visible light and results are displayed in

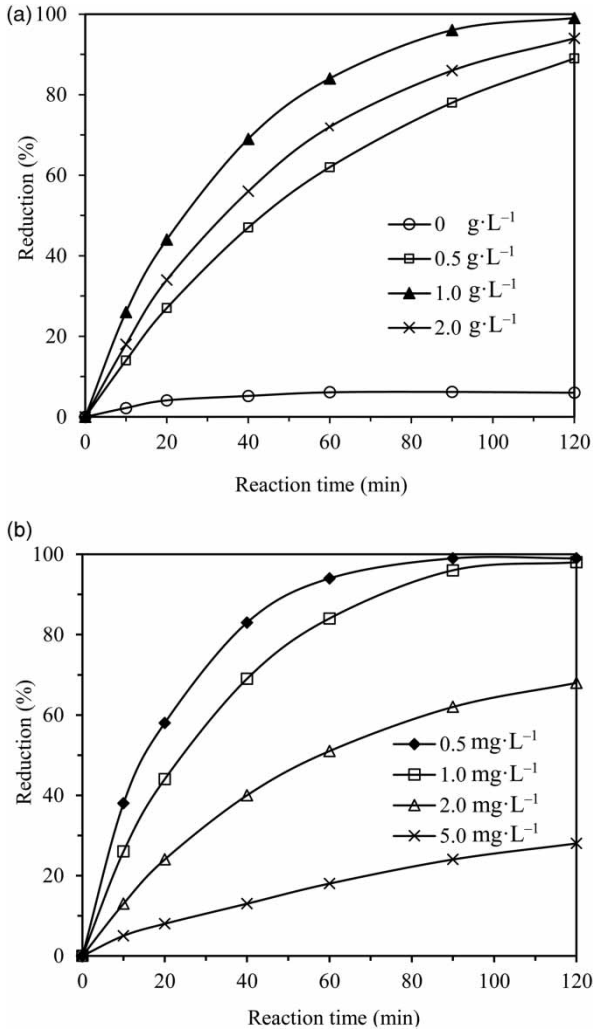

Figure 2 | (a) Effect of TiO_2 dosage on photocatalytic reduction of Cr^{6+} in the presence of air bubbles, where $[Cr_2O_7^{2-}] = 1.0$ mg·L^{-1}, pH = 3, $P = 150$ W; (b) effect of $Cr_2O_7^{2-}$ concentration on photocatalytic reduction of Cr^{6+} in the presence of air bubbles, where $[TiO_2] = 1.0$ g·L^{-1}, pH = 3.0, $P = 150$ W.

Figure 3(a). It is observed that photocatalytic reduction efficiency decreases with the enhancement of pH value. In TiO_2 photocatalytic reduction of Cr^{6+}, pH not only affects the charge property of TiO_2 but also influences the existing form of Cr^{6+} species. Acharya *et al.* (2018) found that the existing form of Cr^{6+} strictly depends on pH value: H_2CrO_4 molecule (pH < 2), $HCrO_4^-$ (2 < pH < 7) and $Cr_2O_7^{2-}$ (pH >7). The isoelectric point of photocatalyst varies depending on preparation conditions, and is particularly affected by pH value (Gumy *et al.* 2006). The isoelectric point of as-prepared TiO_2 was tested using an electrochemical method controlled by a zeta potentiometer and was found to be about 5. The surface of TiO_2 is positively charged when the pH value is lower than 5 and

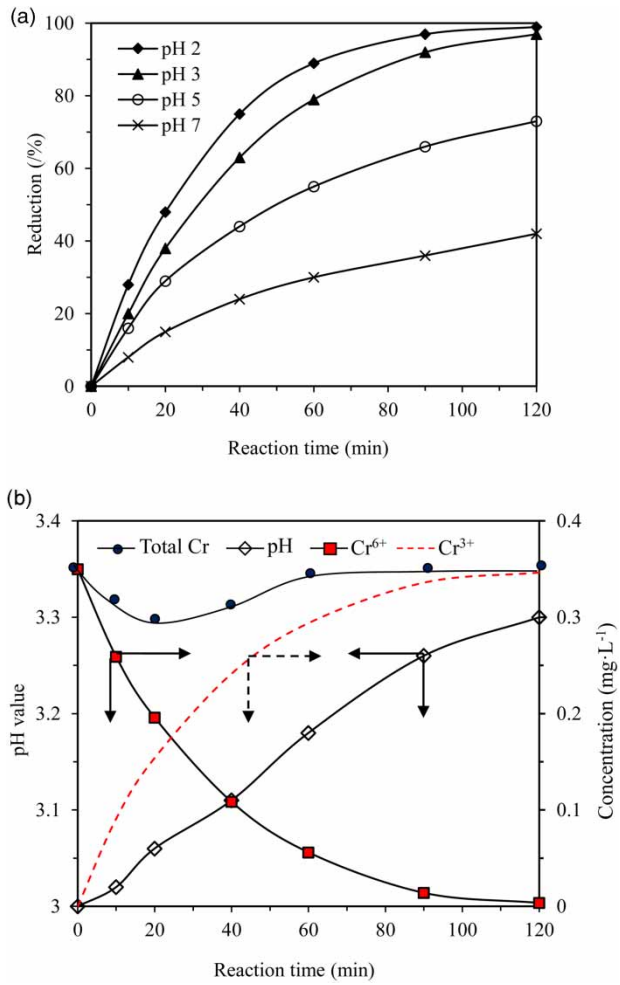

Figure 3 | (a) Effect of pH values on photocatalytic reduction of Cr^{6+} in the presence of air bubbles; (b) the changes of pH, concentration of Cr^{6+}, and Cr^{3+} during photocatalytic reduction, where $[TiO_2] = 1.0\ g{\cdot}L^{-1}$, $[Cr_2O_7^{2-}] = 1.0\ mg{\cdot}L^{-1}$, $P = 150$ W.

negatively charged when the pH value is higher than 5. In TiO_2 photocatalytic reduction, the main form of Cr^{6+} is $HCrO_4^-$ when the pH value ranges from 2 to 5. In this situation, the TiO_2 surface is positive, and more $HCrO_4^-$ anions are adsorbed onto the TiO_2 surface due to coulomb attraction forces when the pH value declines gradually. The adsorbed $HCrO_4^-$ ions are then reduced to Cr^{3+} in situ by reductive substances. When the pH value increases from 5 to 7, the dominant existing form of Cr^{6+} is still $HCrO_4^-$; however, the negative charge property of the TiO_2 surface becomes stronger, which results in the adsorption of $HCrO_4^-$ anions on the catalyst surface and so the photocatalytic reduction declines. Adsorption is a key step for photocatalytic reactions – the stronger the adsorption, the higher the photocatalytic reduction efficiency.

$HCrO_4^-$ ions are reduced to Cr^{3+} in TiO_2 photocatalytic reduction, consuming lots of hydrogen ions, as the following equations demonstrates:

$$3e^- + 7H^+ + HCrO_4^- = Cr^{3+} + 4H_2O \quad \text{(R1)}$$

Figure 3(b) records the changes of pH value and Cr^{6+} concentration. From this figure, it can be seen that the pH value enhances from 3.0 to 3.3 and the Cr^{6+} concentration declines from 0.35 to 0.017 $mg{\cdot}L^{-1}$ after 120 min. The concentration of generated Cr^{3+} ions is 0.35 $mg{\cdot}L^{-1}$ at the same reaction time, theoretically. In fact, the actual Cr^{3+} may be lower than the theoretically concentration because some produced Cr^{3+} is still adsorbed on the TiO_2 surface, as shown by XPS analysis. On the other hand, dissolved Cr^{3+} may be precipitated to $Cr(OH)_3$ by OH^- anions if the mathematical product of Cr^{3+} and $(OH^-)^3$ is higher than the solubility of $Cr(OH)_3$ ($K_{sp} = 6.31 \times 10^{-31}$), as in the following chemical reaction:

$$Cr^{3+} + 3OH^- \rightleftharpoons Cr(OH)_3 \quad \text{(R2)}$$

In this experiment, it is presumed that all $HCrO_4^-$ ions are reduced to Cr^{3+} and released into solution, the maximum concentration of Cr^{3+} reached is at $2/294 \times 10^{-3}$ $mol{\cdot}L^{-1}$ (initial concentration of $K_2Cr_2O_7$ is 1.0 $mg{\cdot}L^{-1}$). At the same time, if the H^+ ions are assumed to be about $2 \times 7/294 \times 10^{-3}$ $mol{\cdot}L^{-1}$ according to Equation (R1), then the OH^- concentration increases to $10^{-14}/(10^{-3} - 2 \times 10^{-3} \times 7/294)$ $mol{\cdot}L^{-1}$ according to the ion product constant of water. The product of Cr^{3+} and $(OH^-)^3$ is 7×10^{-39}, which is much lower than 6.31×10^{-31}. This means that Cr^{3+} cannot be precipitated in the form of $Cr(OH)_3$ in this experiment.

Effect of atmospheres and scavengers

Effects of N_2, O_2, and air bubbles on TiO_2 photocatalytic reductions were studied and the results are shown in Figure 4(a). It is observed that the order of reduction ability of Cr^{6+} is $N_2 >$ air $> O_2$, suggesting that N_2 is positive for reduction and O_2 is negative for it. This is probably because the amount of O_2 molecules consume photoinduced electrons to produce a superoxide radical $\cdot O_2^-$, displayed in the following reaction:

$$O_2 + e \rightarrow \cdot O_2^- \quad \text{(R3)}$$

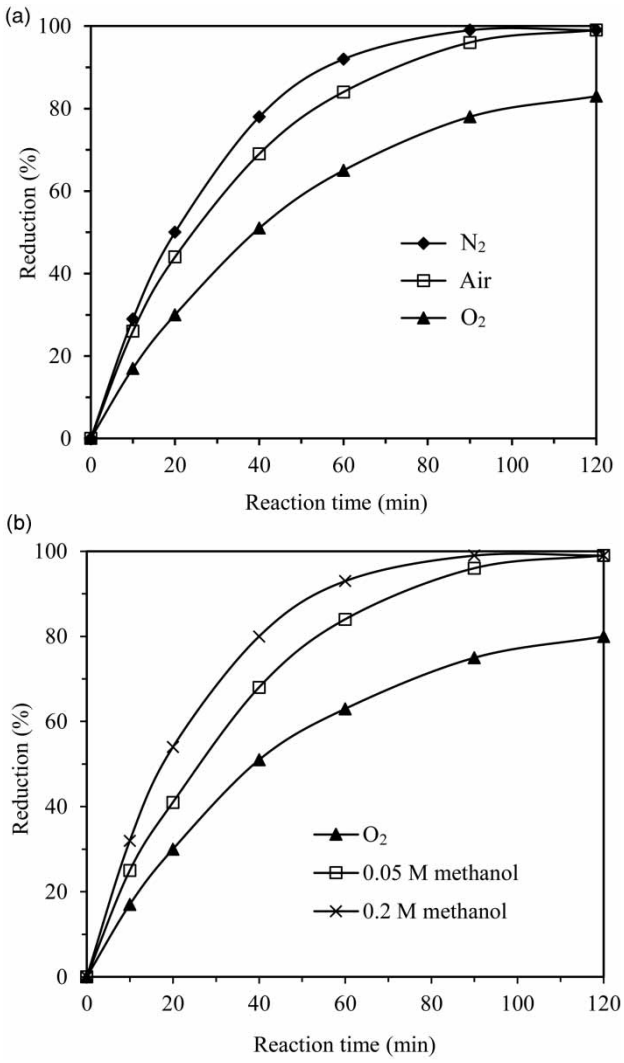

Figure 4 | (a) Effect of N_2, O_2, and air bubbles on photocatalytic reduction of Cr^{6+}; (b) effect of scavengers on photocatalytic reduction of Cr^{6+}, where $[TiO_2] = 1.0\ g{\cdot}L^{-1}$, $[Cr_2O_7^{2-}] = 1.0\ mg{\cdot}L^{-1}$, pH = 3, $P = 150$ W.

The production of $\cdot O_2^-$ aggravates a tense competition between O_2 and Cr^{6+} with photoinduced electrons, and only some of the photoinduced electrons are involved in the reduction of Cr^{6+}, inhibiting photocatalytic reduction efficiency. On the contrary, bubbling N_2 can greatly drive dissolved O_2 which is an effective photoinduced electron scavenger from aqueous solution, and as a result, more photoinduced electrons can take part in the reduction of Cr^{6+} in this situation, compared with those in O_2 or air atmospheres. In fact, oxidation–reduction is a concurrent reaction in the TiO_2 photocatalytic process. In this work, TiO_2 photocatalytic reduction conducted by photoinduced electrons was used to treat Cr^{+6}. A partial oxidation reaction caused by photoinduced holes or hydroxyl radicals occurs, which consumes a lot of photoinduced electrons if there is no additional scavenger of holes, leading to low photocatalytic efficiency.

To inhibit the recombination of photoinduced carriers and deduce photocatalytic reduction pathway, methanol acting as a scavenger of holes was added to system. The influence of methanol on TiO_2 photocatalytic reduction was determined and the results are displayed in Figure 4(b). It is observed that the photocatalytic reduction efficiency of Cr^{6+} increased and it increases with an increase in methanol dosage. Well known, photoinduced holes are easily captured by methanol (Gumy *et al.* 2006), hence more photoinduced electrons can participate in the reduction of Cr^{+6} instead of recombination of carriers, compared with those in the absence of methanol, which verifies that Cr^{6+} is removed via photocatalytic reduction channel.

Photocatalytic reduction mechanism

The $HCrO_4^-$ anion is the dominant existing form when the pH is between 2 and 7. In this situation, adsorption of $HCrO_4^-$ spontaneously happens on the surface of TiO_2, forming a narrow bandgap $HCrO_4/TiO_2$ complex catalyst, which is proven by UV–Vis DRS analysis. Photoinduced electrons are generated on the $HCrO_4^-/TiO_2$ conduction band in visible light irradiation and are involved in the reduction of Cr^{6+}. To verify this hypothesis, XPS and UV–Vis DRS were both conducted and the results are shown in Figure 5. Figure 5(a) displays the XPS spectra of three samples. The first sample is as-prepared TiO_2 powder, named as TiO_2; the second is TiO_2 powder which is soaked in $1.0\ mg{\cdot}L^{-1}$ $Cr_2O_7^{2-}$ aqueous solution for 1 h in dark and then dried at 100 °C, named as TiO_2 before reaction; and the third is TiO_2 powder which is recovered from the reduction system after 120 min, named as TiO_2 after reaction. It is apparent that there are three characteristic peaks in the spectrum of TiO_2 with binding energies of 530.2 eV, 459.5 eV, and 285.7 eV, and they are assigned to O1s, Ti2p, and C1s elements, respectively. The peak of C1s is possibly caused by pollution. It is found that Cr2p intensity in the spectrum of TiO_2 before reaction (blue line) is stronger than that of TiO_2 (black line), suggesting that some $HCrO_4^-$ ions are adsorbed onto the TiO_2 surface in dark conditions. However, it is surprising that the Cr2p peak almost disappears in the spectrum of TiO_2 after reaction (red line), revealing that adsorbed $HCrO_4^-$ ions are reduced under visible light irradiation. Three continuous steps including adsorption, reduction, and desorption are involved in the reduction of Cr^{6+}. These steps continue until almost all $HCrO_4^-$ anions are reduced.

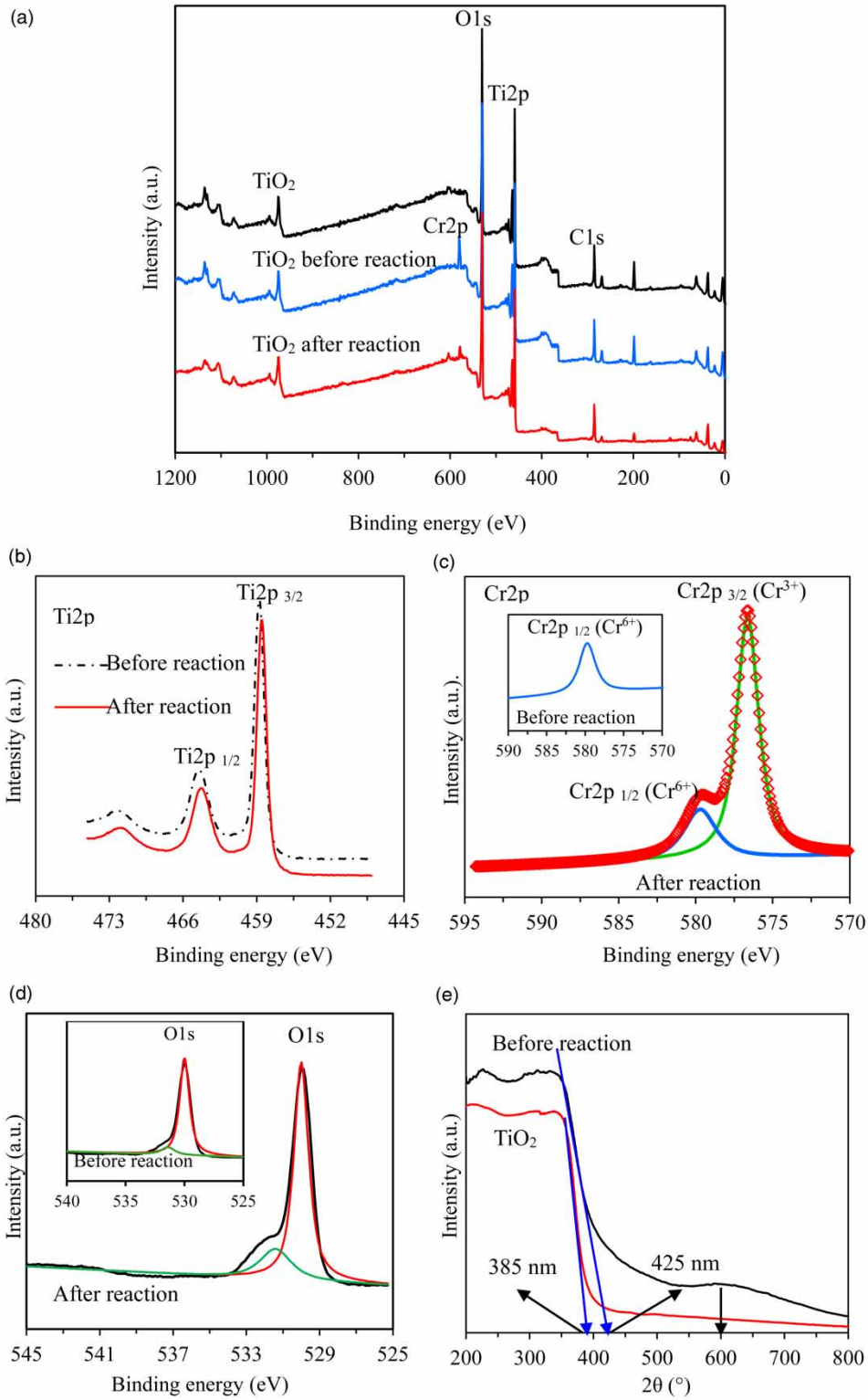

Figure 5 | (a) XPS spectra of three samples (TiO_2, TiO_2 before, and TiO_2 after reaction); (b) Ti2p XPS spectrum and separation peak at the binding energy of 459.5 eV for two samples (TiO_2 before and TiO_2 after reaction); (c) Cr2p XPS spectrum and separation peak at the binding energy of 579.7 eV for the sample (TiO_2 after reaction), and the inset is the Cr2p XPS spectrum of the sample (TiO_2 before reaction); (d) O1s XPS spectra and separation peak at the binding energy of 530.2 eV for two samples of TiO_2 after reaction and TiO_2 before reaction (the inset picture); (e) UV–Vis diffuse reflectance spectra of TiO_2 and TiO_2 before reaction.

The peak of Ti2p binding at 459.5 eV was fitted using XPS software and results are shown in Figure 5(b). One peak appears at the binding energy of 464.4 eV which is caused by $Ti2p_{1/2}$ and the other appears at 458.8 eV which is caused by $Ti2P_{3/2}$. It is found that Ti^{4+} is the only chemical form during the whole photocatalytic reduction, demonstrating that TiO_2 keeps a good structural stability. The fitting of Cr2p binding at 579.7 eV was also analyzed and results are shown in Figure 5(c). The spectrum of Cr2p marked with red diamonds is divided into two individual spectra marked with green and blue curves, respectively. The blue line represents the spectrum of $Cr2p_{1/2}$ and it belongs to Cr^{6+} with a characteristic peak at 579.7 eV. The green line represents the spectrum of $Cr2p_{3/2}$ and is assigned to Cr^{3+} with the characteristic peak at 576.6 eV. It is concluded that Cr^{3+} is the only reductive product. At the same time, the fitting of Cr2p in the spectrum before photocatalytic reaction was simulated, but there is only one $Cr2p_{1/2}$ peak caused by Cr^{6+}, shown in Figure 5(c). This shows that $HCrO_4^-$ is intitially adsorbed on the surface of TiO_2 before photocatalytic reaction and is then reduced in situ to Cr^{3+} in visible light irradiation. The quantities of Cr^{6+} and Cr^{3+} adsorbed on the TiO_2 surface are calculated and exported using software. Molar ratio of Cr^{6+}:Cr^{3+} is about 1:4, indicating that $HCrO_4^-$ is reduced to Cr^{3+} and that Cr^{3+} ions still adsorb on the surface of TiO_2 catalyst. Figure 5(d) displays the fitting of O1s spectra in two samples of TiO_2 after and before reaction (inset figure), respectively. It is observed that O1s binding at 530.2 eV can be divided into two peaks. One peak binding at 530.0 eV (red curve) is assigned to the lattice oxygen coming from TiO_2 and $HCrO_4^-$, and the other binding at about 531.4 eV (green curve) probably belongs to hydroxyl oxygen coming from the chemical adsorption of oxygen, which is in accordance with the conclusion by Yang *et al.* (2006). It is obvious that the hydroxyl oxygen is higher on the TiO_2 surface after the reaction than before reaction, proving that O_2 or OH^- or produced $\cdot O_2^-$ adsorbs on the TiO_2 surface during photocatalytic reduction. Figure 5(e) shows the absorption bandgap of pure TiO_2 and TiO_2 before photocatalytic reaction. The absorption of pure TiO_2 focuses on the ultraviolet zone and that of TiO_2/$HCrO_4^-$ increases to visible light scope, proving that TiO_2/$HCrO_4^-$ can produce photoinduced carriers irradiated by visible light.

Based on the above analysis, visible light-driven TiO_2 photocatalytic reduction of Cr^{6+} was explored. The mechanism involves four major pathways: (1) adsorption of $HCrO_4^-$ on the surface of TiO_2; (2) production of photoinduced electrons under visible light irradiation; (3) reduction of Cr^{6+} to Cr^{3+} by photoinduced electrons; and (4) desorption of Cr^{3+}. The cycle of adsorption → reduction → desorption continues until almost all the $HCrO_4^-$ is reduced.

Life span, kinetics and application

TiO_2 was reused eight times under the same experimental conditions and the results are shown in Figure 6(a). It is observed that the TiO_2 photocatalytic reduction efficiency does not decrease with recycled times, showing that TiO_2 has a satisfied structural stability and a potential application for use in wastewater treatment. Photocatalytic reduction kinetics of Cr^{6+} with TiO_2 was investigated and results are shown in Figure 6(b) and 6(c). The photocatalytic reduction fits well with pseudo-first-order kinetics when $Cr_2O_7^{2-}$ initial concentration ranges from 0.5 to 5.0 $mg{\cdot}L^{-1}$, and rate constants decrease with the enhancement of $Cr_2O_7^{2-}$ initial concentration. The functional relationship between first-order kinetic rate constants and $Cr_2O_7^{2-}$ initial concentration was simulated and shown in Figure 6(c). Pseudo-first-order kinetics constant (k) can be described as: $k = 0.023\ C^{-1.42}$, where C is the $Cr_2O_7^{2-}$ initial concentration. Hence, we can obtain the corresponding k value at a certain $Cr_2O_7^{2-}$ initial concentration according to this simulation.

To investigate the application of TiO_2 photocatalytic reduction in real industrial wastewater containing Cr^{6+}, a small-scale static test was carried out in the same reactor. Properties, including $Cr_2O_7^{2-}$ initial concentration and pH of chemical wastewater, are listed in Table 1, and experimental results are shown in Figure 6(d). It is observed that removal efficiencies of Cr^{6+} in the simulation experiment and small-scale static test are 100% and 93%, respectively, suggesting that TiO_2 photocatalytic reduction can be used to treat wastewater containing Cr^{6+}. The slight decline of Cr^{6+}removal may be caused by co-existing ions in chemical wastewater.

CONCLUSIONS

Almost 100% of Cr^{6+} is reduced to Cr^{3+} in situ by visible light-driven TiO_2 photocatalytic reduction under the optimal experimental conditions. Photoinduced electrons are the major reductive substance of Cr^{6+}, and the mechanism involves adsorption of $HCrO_4^-$, reduction of Cr^{6+}, and desorption of Cr^{3+}. The TiO_2 photocatalyst has a reliable lifespan for reduction Cr^{6+} under visible light irradiation and its

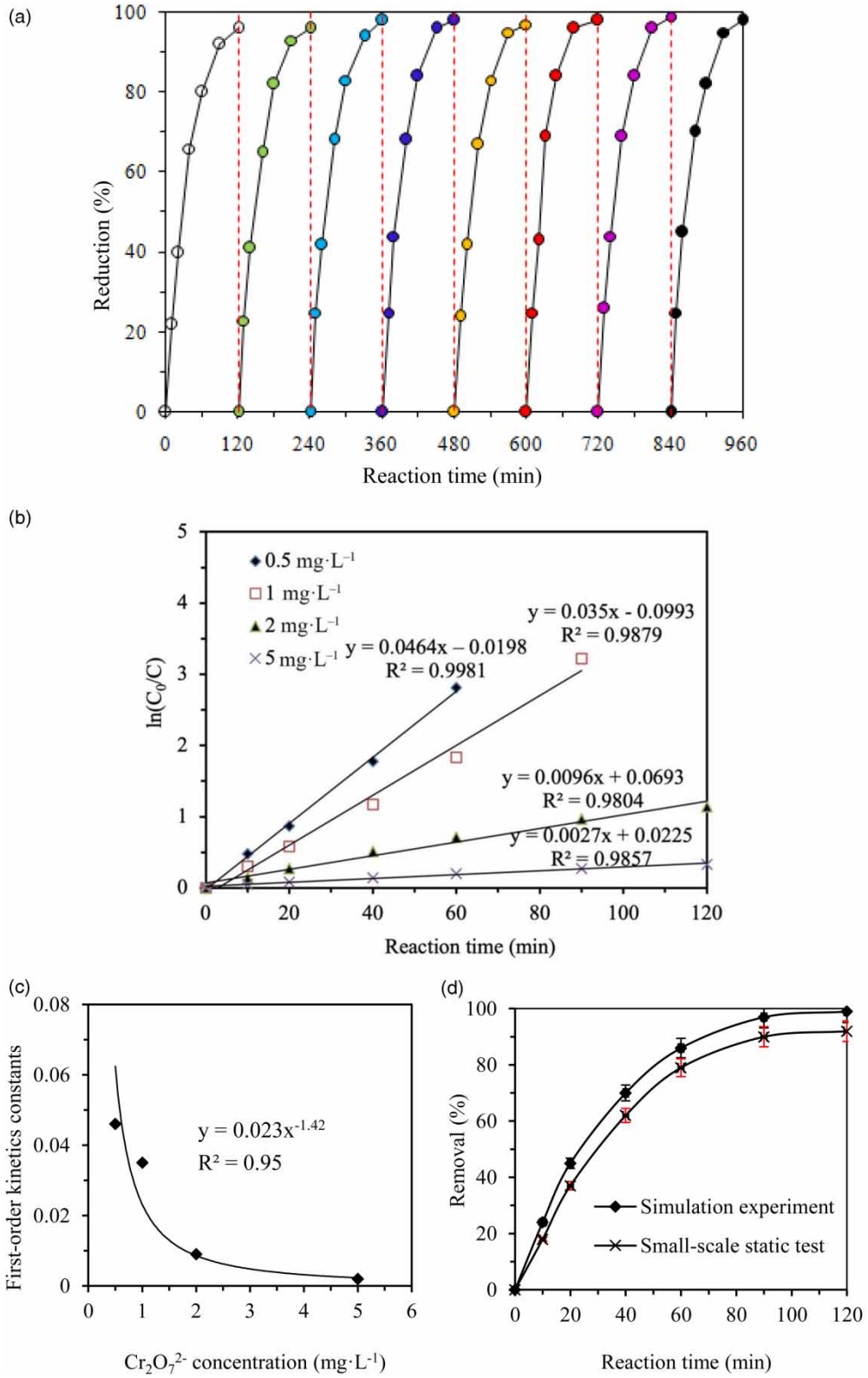

Figure 6 | (a) Life span of TiO_2 photocatalyst of Cr^{6+}; (b) relationship between ln (C_0/C) and reaction time; (c) effect of $Cr_2O_7^{2-}$ initial concentration on first-order kinetics constants; (d) removal of Cr^{6+} in simulation experiment and small-scale static test under the same experiment conditions.

Table 1 | Properties of wastewater

$Cr_2O_7^{2-}$	pH	Turbidity	Temp.	Conductivity	Ca^{2+}	Na^{+}	NO_3^{-}	Cl^{-}
$1\ mg{\cdot}L^{-1}$	5	4	20 °C	$160\ m{\cdot}sm^{-1}$	$10^{-3}\ mg{\cdot}L^{-1}$	$10^{-3}\ mg{\cdot}L^{-1}$	$10^{-3}\ mg{\cdot}L^{-1}$	$10^{-3}\ mg{\cdot}L^{-1}$

photocatalytic reduction reaction fits well with pseudo-first-order kinetics.

ACKNOWLEDGEMENTS

This work is economically funded by Natural Science Foundation of Shandong Province (No: ZR2019MEE097; ZR2016EEM15) and the National Water Pollution Control and Treatment Science and Technology Major Project (No: 2017ZX07101-002-05). Furthermore, we thank Colin Zhao for the revision in English grammar and sentences structure.

DATA AVAILABILITY STATEMENT

All relevant data are included in the paper or its Supplementary Information.

REFERENCES

Acharya, R., Naik, B. & Parida, K. 2018 Cr(VI) remediation from aqueous environment through modified-TiO_2-mediated photocatalytic reduction. *Beilstein Journal of Nanotechnology* **9**, 1448–1470.

Asgari, E., Sheikhmohammadi, A., Nourmoradi, H., Nazari, S. & Aghanaghad, M. 2021 Degradation of ciprofloxacin by photocatalytic ozonation process under irradiation with UVA: comparative study, performance and mechanism. *Process Safety & Environmental Protection* **147**, 356–366.

Ayub, S., Siddique, A. A., Khursheed, M. S., Zarei, A., Alam, I., Asgari, E. & Changani, F. 2020 Removal of heavy metals (Cr, Cu and Zn) from electroplating wastewater by electrocoagulation and adsorption processes. *Desalination & Water Treatment* **179**, 263–271.

Chatterjee, D. & Dasgupta, S. 2005 Visible light induced photocatalytic degradation of organic pollutants. *Journal of Photochemistry and Photobiology C: Photochemistry Reviews C* **6** (2–3), 186–205.

Deveci, H. & Kar, Y. 2013 Adsorption of hexavalent chromium from aqueous solutions by bio-chars obtained during biomass pyrolysis. *Journal of Industrial & Engineering Chemistry* **19** (1), 190–196.

Fujishima, A., Zhang, X. T. & Tryk, D. A. 2008 TiO_2 photocatalysis and related surface phenomena. *Surface Science Reports* **63** (11), 515–582.

Gheju, M. & Balcu, I. 2017 Assisted green remediation of chromium pollution. *Journal of Environmental Management* **203**, 920–924.

Gong, Y., Gai, L., Tang, J., Fu, J., Wang, Q. & Zeng, E. Y. 2017 Reduction of Cr(VI) in simulated groundwater by FeS-coated iron magnetic nanoparticles. *Science of the Total Environment* **595**, 743–751.

Gumy, D., Morais, C., Bowen, P., Pulgarin, C., Giraldo, S., Hajdu, R. & Kiwi, J. 2006 Catalytic activity of commercial of TiO_2 powders for the abatement of the bacteria (*E. coli*) under solar simulated light: influence of theisoelectric point. *Applied Catalysis B Environmental* **63** (1–2), 76–84.

Guo, S. H., Liu, Z. L., Li, Q. S., Yang, P., Wang, L. L., He, B. Y., Xu, Z. M., Ye, J. S. & Zeng, E. Y. 2016 Leaching heavy metals from the surface soil of reclaimed tidal flat by alternating seawater inundation and air drying. *Chemosphere* **157**, 262–270.

Habibi, S., Nematollahzadeh, A. & Mousavi, S. A. 2015 Nano-scale modification of polysulfone membrane matrix and the surface for the separation of chromium ions from water. *Chemical Engineering Journal* **267**, 306–316.

Hoffmann, M., Martin, S. T., Chio, W. & Bahnemann, D. W. 1995 Environmental applications of semiconductor photocatalysis. *Chemical Reviews* **95**, 69–96.

Jobby, R., Jha, P., Yadav, A. K. & Desai, N. 2018 Biosorption and biotransformation of hexavalent chromium [Cr(VI)]: a comprehensive review. *Chemosphere* **207**, 255–266.

Kerkez-Kuyumcu, Ö., Kibar, E., Dayıoğlu, K., Gedik, F., Özkara-Aydınoğlu, Ş., Gedik, F., Akın, A. N. & Zkara-Aydınoglu, S. Ö. 2015 A comparative study for removal of different dyes over M/TiO_2 (M = Cu, Ni, Co, Fe, Mn and Cr) photocatalysts under visible light irradiation. *Journal of Photochemistry & Photobiology A Chemistry* **311**, 176–185.

Magadevan, D., Dhivya, E., Mundari, N. D. A., Mishra, T. & Aman, N. 2019 Development of novel TiO_2-$Cu_2(OH)PO_4$ heterojunction as nanophotocatalyst for improved Cr(VI) reduction. *Journal of Environmental Chemical Engineering* **7** (2), 102968.

Ravindra, K. & Mor, S. 2019 Distribution and health risk assessment of arsenic and selected heavy metals in groundwater of Chandigarh, India. *Environ. Environmental Pollution* **250**, 820–830.

Sarahney, H., Mao, X. & Alshawabkeh, A. N. 2012 The role of iron anode oxidation on transformation of chromium by electrolysis. *Electrochimica Acta* **86**, 96–101.

Sheikhmohammadi, A., Mohseni, S. M., Hashemzadeh, B., Asgari, E., Sharafkhani, R., Sardar, M., Sarkhosh, M. & Almasiane, M. 2019 Fabrication of magnetic graphene oxide

nanocomposites functionalized with a novel chelating ligand for the removal of Cr(VI): modeling, optimization, and adsorption studies. *Desalination & Water Treatment* **160**, 297–307.

Testa, J. J., Grela, M. A. & Litter, M. I. 2004 Heterogeneous photocatalytic reduction of chromium(VI) over TiO_2 particles in the presence of oxalate: involvement of Cr(V) species. *Environmental Science & Technology* **38** (5), 1589–1594.

Vendruscolo, F., Ferreira, R. G. L. & Filho, N. R. A. 2017 Biosorption of hexavalent chromium by microorganisms. *International Biodeterioration & Biodegradation* **119**, 87–95.

Wang, Q., Yang, C., Hang, G. Z., Hu, L. & Wang, P. 2017 Photocatalytic Fe-doped TiO_2/PSF composite UF membranes: characterization and performance on BPA removal under visible-light irradiation. *Chemical Engineering Journal* **319**, 39–47.

Wang, X., Fu, R., Li, H., Zhang, Y., Xiong, Y., Lu, M., Xiao, K., Zhang, X., Zheng, C. & Xiong, Y. 2020 Heavy metal contamination in surface sediments: a comprehensive, large-scale evaluation for the Bohai Sea, China. *Environmental Pollution* **260**, 113986.

Wang, X., Zhang, L., Bu, Y. & Sun, W. 2021 Interplay between invasive single atom Pt and native oxygen vacancy in anatase TiO_2 (101) surface: a theoretical study. *Applied Surface Science* **540**, 148357.

Wu, Q., Zhao, J., Qin, G., Wang, C., Tong, X. & Xue, S. 2013 Photocatalytic reduction of Cr(VI) with TiO_2 film under visible light. *Applied Catalysis B Environmental* **142–143**, 142–148.

Xu, L., Bai, X., Guo, L., Yang, S. & Yang, L. 2019 Facial fabrication of carbon quantum dots (CDs)-modified N-TiO_{2-x} nanocomposite for the efficient photoreduction of Cr(VI) under visible light. *Chemical Engineering Journal* **357**, 473–486.

Yang, S., Zhu, W., Jiang, Z., Chen, Z. & Wang, J. 2006 The surface properties and the activities in catalytic wet air oxidation over CeO_2–TiO_2 catalysts. *Applied Surface Science* **252** (24), 8499–8505.

Yang, Q., Li, Z., Lu, X., Duan, Q., Huang, L. & Bi, J. 2018 A review of soil heavy metal pollution from industrial and agricultural regions in China: pollution and risk assessment. *Science of the Total Environment* **642**, 690–700.

Yao, W., Wang, J., Wang, P., Wang, X., Yu, S., Zou, Y., Hou, J., Hou, J., Hayat, T., Alsaedi, A. & Wang, X. 2017 Synergistic coagulation of GO and secondary adsorption of heavy metal ions on Ca/Al layered double hydroxides. *Environmental Pollution* **229**, 827–836.

Yoshinaga, M., Ninomiya, H., Al Hossain, M. M. A., Sudo, M., Akhand, A. A., Ahsan, N., Alim, M. A., Khalequzzaman, M., Iida, M., Yajima, I., Ohgami, I. N. & Kato, M. 2018 A comprehensive study including monitoring, assessment of health effects and development of a remediation method for chromium pollution. *Chemosphere* **201**, 667–675.

Yu, X., Yu, R. Q., Gui, D., Zhang, X. & Wu, Y. 2018 Hexavalent chromium induces oxidative stress and mitochondria-mediated apoptosis in isolated skin fibroblasts of Indo-Pacific humpback dolphin. *Aquatic Toxicology* **203**, 179–186.

Zhang, C., Xia, F., Long, J. & Peng, B. 2017 The pollution of chromium in wet-end process of leather manufacture. *Journal of Cleaner Production* **154**, 276–283.

Zhao, B., Lv, M. & Zhou, L. 2012 Photocatalytic degradation of perfluorooctanoic acid with beta-Ga_2O_3 in anoxic aqueous solution. *Journal of Environmental Science* **24** (4), 774–780.

Zhao, B., Li, X., Li, W., Yang, L., Li, J., Xia, W., Zhou, L. & Zhao, C. 2015 Degradation of trichloroacetic acid by an efficient Fenton/UV/TiO_2 hybrid process and investigation of synergetic effect. *Chemical Engineering Journal* **273**, 527–533.

Zhao, B., Wang, X., Shang, H., Li, X., Li, W., Li, J., Xia, W., Zhou, L. & Zhao, C. 2016 Degradation of trichloroacetic acid with an efficient Fenton assisted TiO_2 photocatalytic hybrid process: reaction kinetics, byproducts and mechanism. *Chemical Engineering Journal* **289**, 319–329.

Zhou, X., Korenaga, T., Takahashi, T., Moriwake, T. & Shinoda, S. 1993 A process monitoring/controlling system for the treatment of wastewater containing chromium (VI). *Water Research* **27** (6), 1049–1054.

First received 29 December 2020; accepted in revised form 14 March 2021. Available online 26 March 2021